Nigerian Journal of Pharmaceutical and Biomedical Research
Vol. 10 Issue.2 August, 2026. p-ISSN: 2579-1419 e-ISSN: 2814-1423

CUO NANOPARTICLES: MEROPENEM POTENTIATION AND EFFLUX-ASSOCIATED RESPONSES *IN KLEBSIELLA PNEUMONIAE* AND *PSEUDOMONAS AERUGINOS*

Intisar Hameed Ali Al-Abdali
Ministry of Education, General Directorate of Education in Anbar
Corresponding email: amsayf77@gmail.com DOI 10.5281/zenodo.23962658.
Intessar.Hameed1102a@ihcoedu.uobaghdad.edu.iq

ABSTRACT

Background: Efflux systems and carbapenemases contribute to antibiotic resistance in Klebsiella pneumoniae and Pseudomonas aeruginosa. Sub-inhibitory CuO nanoparticles may modify efflux-associated responses and antibiotic susceptibility. **Objectives:** To assess antibiotic potentiation and efflux-associated responses to sub-inhibitory CuO nanoparticles in clinical isolates of both species, and to compare the effects of the antibiotic partner and bacterial species. **Methods:** One hundred twenty clinical isolates (60 per species) underwent susceptibility, carbapenemase, EtBr retention, transcriptional, biofilm and cytotoxicity analyses. Mechanistic CuO exposure was 0.25 × the isolate-specific MIC. Antibiotic interaction analyses used the recorded point-specific combination endpoints and separate 4 × 4 response matrices, with explicit FICI, Bliss and highest-single-agent (HSA) calculations. Correlations were assessed for the pooled cohort and separately within each species. Twenty-four-hour additional killing was recalculated from isolate-level log10 CFU/mL endpoints. Continuous outcomes are median (IQR), unless specified as means; categorical outcomes are n/N (%). **Results:** Meropenem, ciprofloxacin and CuO minimum inhibitory concentrations did not differ significantly between species (P = 0.920, 0.409 and 0.545, respectively). blaKPC and blaOXA-48 occurred only in K. pneumoniae, in 26/60 (43.3%) and 33/60 (55.0%) isolates, respectively, and blaVIM occurred only in P. aeruginosa, in 30/60 (50.0%) isolates (all P < 0.001). Recorded point-specific FICI values met the synergy threshold with meropenem in 56/60 (93.3%) K. pneumoniae and 59/60 (98.3%) P. aeruginosa isolates, compared with 39/60 (65.0%) and 41/60 (68.3%), respectively, with ciprofloxacin (pooled exact McNemar P < 0.001). The median FICI for both species was 0.375 (IQR 0.375–0.500) for meropenem. Median ethidium bromide accumulation increases were 242.2% (IQR 176.6–300.0%) and 265.7% (IQR 218.4–328.7%) in K. pneumoniae and P. aeruginosa, respectively. All eight efflux-associated targets had lower cohort median expression; gene-specific median fold changes ranged from 0.331 to 0.431 (Holm-adjusted P < 0.001 for each target), with discordant individual isolates. Median biofilm inhibition was 66.92% (IQR 61.39–72.04%) and 73.62% (IQR 67.36–77.99%), respectively. The meropenem combination resulted in median additional reductions at 24 h relative to the more active single agent of 2.306 (IQR 2.286–2.335) and 2.295 (IQR 2.270–2.328) log10 CFU/mL, respectively. Median curve-specific CC50 estimates were 365.96 (IQR 186.48–476.22) and 383.22 (IQR 215.20–492.90) µg/mL, with median MIC-normalised CC50/(0.25 × CuO MIC) ratios of 6.30 (IQR 5.57–7.09) and 6.18 (IQR 5.46–7.17), respectively. Mean cell viability was 94% at 0.25 × MIC, and 119/120 (99.2%) isolates had a ratio above 1. Within-species EtBr–gene-expression correlations were −0.890 and −0.900, and EtBr–biofilm-inhibition correlations were 0.861 and 0.947, respectively (all Holm-

adjusted P < 0.001). **Conclusions:** More recorded meropenem FICI values met the synergy threshold than ciprofloxacin values, while median additional killing at 24 h was similar. The recorded FICI points were not independently validated as whole-checkerboard classifications. Associations of EtBr retention with gene expression and biofilm inhibition remained strong within both species. Meropenem FICI associations were significant within K. pneumoniae but not P. aeruginosa; ciprofloxacin associations had the opposite direction in the pooled heatmap. These findings do not establish a uniform efflux-mediated mechanism. MIC-normalised cytotoxicity ratios do not establish a clinical safety margin.
Keywords: copper oxide nanoparticles; efflux pump inhibition; carbapenem resistance; *Klebsiella pneumoniae; RND efflux pumps; antimicrobial synergy*

1. INTRODUCTION

Antimicrobial resistance is no longer a forecast; it is a measured burden. In 2021, 1.14 million deaths were directly attributable to bacterial resistance and 4.71 million were associated with it, and mortality among people aged 70 and above rose by more than 80% between 1990 and 2021 (GBD 2021 An*timicrobial Resistance Collaborators,* 2024). The World Health Organization's 2024 Bacterial Priority Pathogens List covers 24 pathogens across 15 families, with carbapenem-resistant Enterobacterales among those of critical priority and carbapenem-resistant *P. aeruginosa* among those of high priority (Sati *et al.,* 2025; Mudenda *et al.,* 2025). The distribution of that burden is uneven. In the WHO African region alone, 1.05 million deaths (95% UI 829,000–1,316,000) were associated with bacterial resistance and 250,000 (192,000–325,000) were attributable to it, with *K. pneumoniae* among four pathogens each responsible for more than 100,000 associated deaths (Sartorius *et al.,* 2024). The clinical response has lagged behind the epidemiological signal.

Efflux contributes to resistance alongside other mechanisms. MexAB-OprM contributes to resistance in P. aeruginosa, regulated by the repressors, namely, mexR, nalC and nalD, and exports macrolides, quinolones, most β-lactams, tetracyclines, chloramphenicol and lincomycin, with a large degree of overexpression observed in carbapenemase-producing carbapenem-resistant isolates (Gauba & Rahman, 2023). The tripartite AcrAB–TolC system is the archetypal RND pump, which is regulated by upregulation of the AraC/XylS activator RamA, resulting in an increased expression of acrAB and tolC and abundance of the pump (Han et al., 2022). The result is in line with the occurrence in clinical surveys, which reveals that efflux-associated genes (acrAB and tolC) and porin genes (ompK35 and ompK36) are frequently found in multidrug-resistant K. pneumoniae and contribute to enhancing the resistance of the isolates (Hussein et al., 2024).

Efflux is more important than just drug extrusion. Nowadays, it is known that biofilm tolerance and efflux are closely related and that there is a synergy between these two mechanisms that enable the development of resistance in the biofilm community

(Vareschi et al., 2025). Efflux is also a mechanism of persistence: β-lactam-tolerant E. coli persisters exhibit reduced drug accumulation, have increased expression of tolC, acrA and acrB and deleting acrB reduces persister survival (Garcia-Maset et al., 2025). Pumps also play an important role in the maturation of the biofilm, meaning that disrupting the pumps will lead to reduced adhesion and maturation, which makes efflux an unusually cost-effective target (Hajiagha & Kafil, 2023). A single treatment might make bacteria sensitive to antibiotics, and make it easier to break down the barriers that keep them protected.

CuO nanoparticles were selected because membrane interactions, reactive oxygen species generation and copper-ion release provide plausible routes to antibiotic potentiation (Gudkov et al., 2024; Modi et al., 2023). CuO combined with chloramphenicol has also been associated with reduced mexA gene expression in resistant P. aeruginosa (Alazavi et al., 2022). These findings provide a rationale for investigating CuO; Ag, ZnO and TiO2 were not tested in this study, and no comparative superiority is claimed. Nanoparticle and nanocarrier strategies targeting efflux-associated determinants are discussed in recent reviews (Thillai et al., 2025; Mbara et al., 2026).

Two obstacles temper this promise. First, no efflux-pump inhibitor has reached clinical use, for reasons of formulation, toxicity, pharmacokinetics or narrow spectrum of inhibition (Duffey *et al.,* 2024); efflux remains difficult to detect and to counteract in clinical settings, and no standardised methods exist to diagnose or inhibit it (Rouvier *et al.,* 2025). Second, findings from individual nanoparticle formulations require assessment across clinical isolates; the present study evaluates two species using the same CuO preparation.

We examined 120 clinical isolates of *K. pneumoniae* and *P. aeruginosa* in parallel, linking combination-MIC and response-matrix measurements with eight efflux-associated transcriptional targets, EtBr retention, biofilm inhibition and killing outcomes in the same isolates. The questions were whether mechanistic responses at 0.25 × MIC differed between species, whether the antibiotic partner influenced interaction outcomes, and how those outcomes related to efflux-associated endpoints. Cell viability was evaluated across MIC-normalised CuO exposure levels; these measurements were not designed to establish an isolate-independent clinical safety margin.

2. Materials and Methods

2.1 Bacterial isolates

One hundred twenty non-duplicate clinical isolates (60 *K. pneumoniae*, 60 *P. aeruginosa*) were obtained from the routine diagnostic microbiology laboratory of Fallujah General Hospital, Fallujah, Al-Anbar, Iraq, between 3 June 2023 and 12 November 2024. All had been reported as multidrug resistant in routine testing; this designation does not imply

resistance to every antibiotic. The cohort was not uniformly meropenem resistant: Kp_29 had a low reported meropenem MIC and was retained; clinical breakpoint interpretation requires verification of the final assay inoculum. Duplicates were discarded. Each isolate was purified to a single colony, stored at −80 °C and used for no more than two passages. A permanent identifier (Kp_01–Kp_60; Pa_01–Pa_60) linked every phenotypic, molecular and functional measurement to the same isolate, and each isolate came from a different patient, so no patient contributed more than one isolate. Species identity was confirmed by MALDI-TOF mass spectrometry, with discordant spectra resolved by 16S rRNA gene sequencing. Primary isolation and presumptive identification of the study isolates are shown in Figure S1.

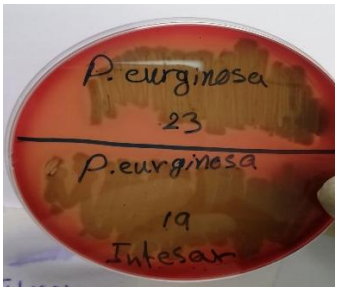

S1: Blood agar plate showing colonial growth of two clinical *P. aeruginosa* isolates.

2.2 Nanoparticle preparation and characterisation

A single lot of CuO nanoparticles was used throughout and was characterised by X-ray diffraction, transmission electron microscopy, dynamic light scattering and zeta-potential analysis. XRD confirmed a monoclinic CuO crystalline phase. TEM showed predominantly spherical particles of approximately 20–40 nm with a typical size of about 28 nm and no agglomeration evident in the dried TEM preparations; dynamic light scattering, performed in sterile distilled water at a nanoparticle concentration of 50 µg/mL, gave a hydrodynamic diameter of 242 ± 96 nm and a polydispersity index of 0.29, and the zeta potential was −15.4 mV, indicating limited colloidal stability. The larger hydrodynamic diameter relative to the TEM size is consistent with hydration and clustering in aqueous suspension (Blinov *et al.,* 2022), however, this size difference alone does not establish the hydrodynamic diameter during exposure in Mueller–Hinton broth, where medium-dependent agglomeration can alter nanoparticle behaviour. The stock suspension was prepared in sterile distilled water using bath sonication for 15 min; working suspensions were prepared fresh on the day of each experiment. The bacterial mechanistic assays used CuO at 0.25 × the isolate-specific MIC; the cytotoxicity assays used a broader MIC-normalised exposure series. The bacterial exposure was sub-inhibitory by MIC, but this does not exclude direct

stress, membrane effects or copper-ion contributions.

2.3 Susceptibility testing and carbapenemase detection

MICs of meropenem, ciprofloxacin and CuO nanoparticles were determined in parallel for every isolate by broth microdilution in cation-adjusted Mueller–Hinton broth in 96-well plates. The reported inoculum preparation was adjustment to 0.5 McFarland followed by a 1:1000 dilution. This description does not establish a final in-well inoculum of approximately 5 × 10^5 CFU/mL, the reference broth-microdilution target (EUCAST, 2024). Using an approximate starting density of 1.5 × 10^8 CFU/mL, the dilution would give 1.5 × 10^5 CFU/mL before any further dilution in the well; equal-volume mixing would reduce this to approximately 7.5 × 10^4 CFU/mL. These are nominal calculations, not measured viable counts. Plates were incubated at 37 °C for 18–24 h. Three recorded MIC determinations were available for each agent and isolate; the final MIC matched the modal value of those entries. This is distinct from a mode calculated from two discordant measurements. *Escherichia coli* ATCC 25922 and *P. aeruginosa* ATCC 27853 served as quality-control strains. Carbapenemase genes *bla*KPC, *bla*NDM, *bla*VIM and *bla*OXA-48 were detected by PCR, and carbapenemase activity was screened by the Modified Hodge test. Primer sequences and expected amplicon sizes are provided in Supplementary Table S1.

2.4 Antibiotic interaction assays and response-matrix analysis

Point-specific combination endpoints and percent-inhibition response matrices were analysed as distinct datasets. Each recorded FICI represents one reported concentration pair; the data do not establish whether that pair was selected as the minimum or maximum FICI across all inhibitory wells. Accordingly, the reported categories are descriptive threshold labels for these recorded points, rather than independently verified whole-checkerboard classifications. For combination MICs, FICI = (antibiotic MIC in combination/antibiotic MIC alone) + (CuO concentration in combination/CuO MIC alone). The recorded CuO fractions were 0.125, 0.25, 0.5, 1 or 2.25 for meropenem, and 0.125, 0.25, 0.5 or 1 for ciprofloxacin. These combination endpoints were not all obtained at fixed 0.25 × MIC CuO. The descriptive FICI thresholds were synergy (≤ 0.5), additive (> 0.5 to ≤ 1), indifference (> 1 to ≤ 4), and antagonism (> 4). For Kp_14, meropenem 64/32 µg/mL and CuO 576/256 µg/mL give FICI = 2.00 + 2.25 = 4.25; the CuO fraction is above MIC and is not the 0.25 × MIC mechanistic exposure. Separately, each SF response matrix contained antibiotic and CuO levels of 0, 0.25, 0.5 and 1 × their respective MICs. With observed percentage inhibition E_AC and matched single-agent responses E_A and E_C, Bliss expected inhibition = E_A + E_C − E_AE_C/100, and HSA expected inhibition = max(E_A, E_C). The score at each combination was observed minus expected inhibition,

expressed in percentage points. Each isolate's summary score was the arithmetic mean over the nine positions with both agents present; the zero-dose margins supplied single-agent controls and were excluded from this mean. No additional baseline correction or fitted response surface was used. The 4 × 4 grid lacks the 0.125 × MIC level present in many recorded FICI pairs and cannot produce Kp_14's 2.00 + 2.25 pair: its maximum possible concentration-fraction sum is 2.00. Moreover, single-agent matrix entries labelled 1 × MIC show approximately 63–66% antibiotic inhibition and 56–59% CuO inhibition, rather than a demonstrated MIC endpoint. The matrix readout therefore cannot validate the separately recorded combination MICs; equivalence of assay conditions and inhibition endpoints was not established. FICI was not calculated from these matrices. These reference models give different expected responses and should not be treated as interchangeable synergy classifications (Ianevski et al., 2022).

2.5 Efflux activity and gene expression

Ethidium bromide accumulation was measured by real-time fluorometry under three conditions: untreated control, 0.25 × MIC CuO, and the reference protonophore carbonyl cyanide m-chlorophenylhydrazone. Fluorescence was recorded at excitation and emission wavelengths of 530 and 585 nm, respectively, in phosphate-buffered saline (PBS; pH 7.4) supplemented with 0.4% (w/v) glucose. Measurements were collected every minute for 60 min at the reported temperature of 40 °C. Responses are interpreted only under this assay condition; a temperature-matched validation or comparison with 37 °C was not reported. Higher fluorescence reflects greater net intracellular EtBr retention, which is compatible with reduced efflux but can also be affected by uptake and membrane permeability (Sobhanipoor *et al.,* 2022; Modi *et al.,* 2023). Total RNA was extracted using the TaKaRa MiniBEST Universal RNA Extraction Kit (Takara Bio). Complementary DNA was synthesised using the PrimeScript RT Reagent Kit with gDNA Eraser (RR047A, Takara Bio). Genomic DNA was removed at 42 °C for 2 min, followed by reverse transcription at 37 °C for 15 min and enzyme inactivation at 85 °C for 5 s; cDNA was held at 4 °C until use. Quantitative real-time PCR was performed using TB Green Premix Ex Taq II (RR820A, Takara Bio), with initial denaturation at 95 °C for 30 s, followed by 40 cycles of 95 °C for 5 s and 60 °C for 30 s. Melting-curve analysis was performed to assess amplification specificity. Relative expression of *acrA*, *acrB*, *tolC* and *ramA* (*K. pneumoniae*) and *mexA*, *mexB*, *oprM* and *mexR* (*P. aeruginosa*) was quantified by qRT-PCR with *rpoB* as *the* reference gene for K. pneumoniae and rpoD for P. aeruginosa. Fold change was calculated by the 2^−ΔΔCt method, and statistical inference was performed on ΔCt values with Holm correction for multiplicity. Primer sequences and species-specific reference genes are provided in Supplementary Table S2.

2.6 Biofilm, time-kill and cytotoxicity assays

Biofilm inhibition was quantified by crystal violet assay after 24 h. The time-kill dataset recorded one log10 CFU/mL endpoint per isolate and condition at 0, 4, 8, 12 and 24 h for control, antibiotic, CuO and combination. Additional killing at 24 h was recalculated as min(log10 CFU/mL antibiotic alone, log10 CFU/mL CuO alone) minus log10 CFU/mL combination. The prespecified synergy threshold was ≥ 2 log10 CFU/mL. These values do not document independent experimental repeat counts or the actual time-kill drug doses. Cytotoxicity was assessed in THP-1-derived human macrophage-like cells using Alamar Blue. The human cell model was the same across experiments; the CuO concentration series was defined relative to each bacterial isolate's MIC. CC50 values are curve-specific estimates obtained under different MIC-normalised exposure grids, not intrinsic properties of bacterial isolates or directly observed tested doses. The recorded CC50 parameters were retained without refitting; the original fitting procedure and parameter uncertainty were not documented. Each CC50 was checked against the maximum tested concentration in its series. Five estimates exceeded that maximum and therefore require extrapolation; they were retained as exploratory estimates and are not experimentally bracketed CC50 measurements. The MIC-normalised concentration ratio was calculated as CC50/(0.25 × CuO MIC). It is a design-dependent concentration ratio and is not an independently established therapeutic safety margin.

2.7 Statistical analysis

Analyses used Python 3.12.14, NumPy 2.3.5 and SciPy 1.17.0. The isolate was the analysis unit. Means of the three recorded EtBr and biofilm readings, and Ct-derived fold changes, were checked against their component values; legacy summary columns were not substituted for these detailed fields. Between-species comparisons used two-sided Mann–Whitney U tests for MIC, FICI, biofilm inhibition, additional killing and cytotoxicity outcomes, and Fisher's exact tests for categorical profiles. Paired continuous antibiotic outcomes and ΔCt comparisons used two-sided Wilcoxon signed-rank tests; differences were rounded to 12 decimal places to avoid floating-point tie artefacts. The paired proportions classified as synergistic with meropenem versus ciprofloxacin were compared across the pooled cohort using the two-sided exact McNemar test. The 43 discordant pairs comprised 39 isolates synergistic only with meropenem and four synergistic only with ciprofloxacin (P = 3.11 × 10^−8). EtBr species contrasts used Welch tests separately by condition. Treatment-by-species differences in EtBr were assessed using a two-degree-of-freedom Wald test of the mean CuO–control and CCCP–control contrasts with their within-isolate covariance. Biofilm optical-density change was compared between species using a Welch test. Spearman coefficients were calculated for the pooled cohort and separately for each species. Holm correction covered the eight gene tests

and, separately, the 24 correlation tests (eight pairs in three groups). Quartiles were calculated by linear interpolation at the 25th and 75th percentiles. Data are mean ± SD or median (IQR); $P < 0.05$ was the significance threshold.

3. Results

3.1 Antimicrobial susceptibility and carbapenemase genotype

The two species were phenotypically comparable and genotypically distinct. Median meropenem MIC was 32 (16–64) µg/mL in both species (P = 0.920); median ciprofloxacin MIC was 32 (16–32) µg/mL in *K. pneumoniae* and 16 (14–32) µg/mL in *P. aeruginosa* (P = 0.409); and median CuO MIC was 256 (128–256) µg/mL in both (P = 0.545). None of the three agents differed significantly between species.

Carbapenemase carriage diverged. *bla*KPC was detected in 26 *K. pneumoniae* isolates (43.3%) and in no *P. aeruginosa* isolate, and *bla*OXA-48 in 33 *K. pneumoniae* isolates (55.0%) and in no *P. aeruginosa* isolate (both $P < 0.001$). *bla*VIM was restricted to *P. aeruginosa*, where it occurred in 30 isolates (50.0%) ($P < 0.001$). Only *bla*NDM was shared, in 33 *K. pneumoniae* (55.0%) and 29 *P. aeruginosa* (48.3%) isolates (P = 0.584). The Modified Hodge test was positive in 59 isolates of each species (98.3%; P = 1.000). Comparable MICs therefore concealed divergent resistance architectures.

Table 1. Antimicrobial susceptibility and carbapenemase profile

Parameter	K. pneumoniae (n = 60)	P. aeruginosa (n = 60)	P value
Meropenem MIC (µg/mL)	32 (16–64); mode 32	32 (16–64); mode 16	0.920
Ciprofloxacin MIC (µg/mL)	32 (16–32); mode 16	16 (14–32); mode 16	0.409
CuO nanoparticle MIC (µg/mL)	256 (128–256); mode 128/256	256 (128–256); mode 256	0.545
blaKPC positive	26 (43.3%)	0 (0.0%)	9.16E−10
blaNDM positive	33 (55.0%)	29 (48.3%)	0.584
blaVIM positive	0 (0.0%)	30 (50.0%)	1.39E−11
blaOXA-48 positive	33 (55.0%)	0 (0.0%)	4.82E−13
Modified Hodge test positive	59 (98.3%)	59 (98.3%)	1.000

Values in Table 1 are median (IQR), with modes where shown, or n (%). P values compare the species using two-sided Mann–Whitney U tests for MICs and two-sided Fisher's exact tests for categorical outcomes. For all three agents, meropenem, ciprofloxacin and CuO nanoparticles, the MIC distributions of the two species were similar, with no statistically significant

differences between them (all P > 0.40). Species-specificity was a major determinant for the molecular resistance profile. blaVIM was only found in P. aeruginosa but not in K. pneumoniae, while blaOXA-48 and blaKPC were only identified in isolates of K. pneumoniae. blaNDM was seen in both species at similar rates. In each species, all but one of the isolates were modified Hodge-positive. These results indicate that similar phenotypic MICs can be seen with very different carbapenemase-gene backbones and that genotype and phenotype must thus be used as complementary, not interchangeable, tools.

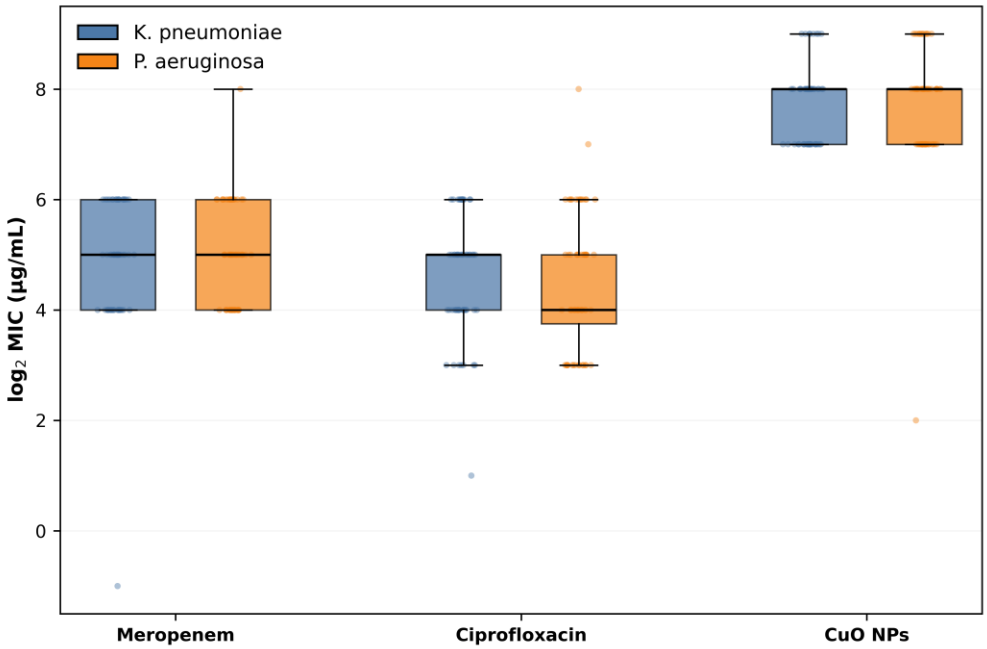

Figure 1. Distribution of meropenem, ciprofloxacin and CuO nanoparticle MIC values according to bacterial species.

The MIC distributions overlapped between species, consistent with the non-significant comparisons in Table 1. Kp_29 had low meropenem and ciprofloxacin MICs, Pa_07 had a high meropenem MIC, and Pa_33 had a low CuO MIC. These retained observations show susceptibility heterogeneity; the cohort should not be described as uniformly meropenem resistant.

3.2 Synergy profiling

Recorded meropenem FICI values .were lower than ciprofloxacin values Median meropenem FICI was 0.375 in both species, with 56 (0.500–0.375) .K. pneumoniae (93.3%) and 59 P aeruginosa (98.3%) recorded points .meeting the synergy threshold. One K pneumoniae value exceeded the .antagonism threshold and one P aeruginosa value fell in the indifferent range. Median ciprofloxacin FICI was and (%65.0) 39 ;(0.750–0.375) 0.500 points met the synergy (%68.3) 41 threshold, and 21 (35.0%) and 18 .fell in the additive range (%30.0) Paired comparison showed an antibiotic-associated difference in recorded FICI (P < 0.001), with no .significant between-species difference Kp_14 had a recorded meropenem

FICI of 4.25 at meropenem 2 × MIC and CuO 2.25 × MIC. This point lies outside the response-matrix grid and does not establish antagonism at sub-inhibitory CuO or across an entire .checkerboard

Table 2. Descriptive categories of recorded FICI points and separate response-matrix scores

Combination	Species	FICI median (IQR)	Synergy	Additive	Indifferent	Antagonism	Bliss median (IQR)	HSA median (IQR)
CuO + Meropenem	K. pneumoniae	0.375 (0.375–0.500)	56 (93.3%)	3 (5.0%)	0 (0.0%)	1 (1.7%)	7.54 (7.18–7.97)	23.87 (23.53–24.34)
CuO + Meropenem	P. aeruginosa	0.375 (0.375–0.500)	59 (98.3%)	0 (0.0%)	1 (1.7%)	0 (0.0%)	7.55 (7.16–8.02)	24.05 (23.50–24.39)
CuO + Ciprofloxacin	K. pneumoniae	0.500 (0.375–0.750)	39 (65.0%)	21 (35.0%)	0 (0.0%)	0 (0.0%)	7.15 (2.89–7.93)	23.60 (19.03–24.30)
CuO + Ciprofloxacin	P. aeruginosa	0.500 (0.375–0.750)	41 (68.3%)	18 (30.0%)	1 (1.7%)	0 (0.0%)	7.38 (3.30–7.82)	23.69 (19.64–24.08)

Applying the stated thresholds to the recorded FICI points reproduced the category counts: 56/60 and 59/60 with meropenem, versus 39/60 and 41/60 with ciprofloxacin, in K. pneumoniae and P. aeruginosa, respectively. The pooled paired difference in synergy proportions was significant by the exact McNemar test ($P < 0.001$). These classifications use the actual CuO concentrations recorded for the combination endpoints, not a uniformly fixed CuO dose. Bliss and HSA summaries were independently reproduced by averaging observed-minus-expected inhibition over the nine joint-treatment cells of each matrix. Pooled paired Wilcoxon comparisons favoured meropenem for FICI, Bliss and HSA (each $P < 0.001$); HSA scores were larger because its reference expectation differs from Bliss. The category counts describe selected recorded endpoints, not a verified minimum/maximum FICI selection over inhibitory wells. Bliss and HSA use a different readout and concentration grid and do not validate those categories. These summaries do not establish therapeutic superiority.

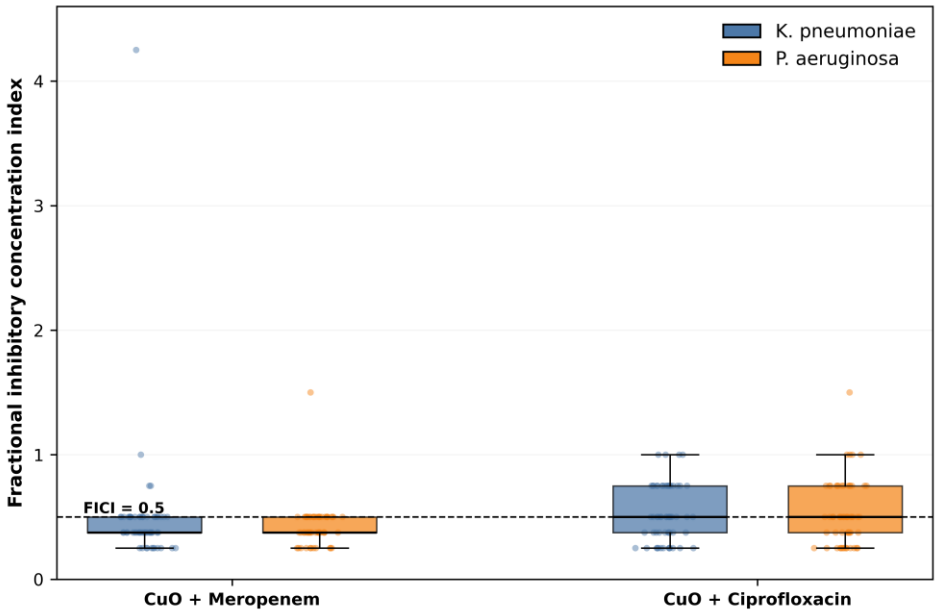

Figure 2. Distribution of recorded point-specific FICI values for CuO–meropenem and CuO–ciprofloxacin. Values are not FICI minima or maxima independently verified across complete checkerboards.

Most recorded meropenem FICI points met the ≤ 0.5 threshold, while ciprofloxacin points more often fell in the additive range. Kp_14 was an outlying meropenem point at 2 × MIC meropenem and 2.25 × MIC CuO. Pa_48 had a meropenem FICI of 1.50, whereas Pa_59 had a meropenem FICI of 0.50 and a ciprofloxacin FICI of 1.50. These descriptive differences do not establish responses at a common CuO concentration or validate a whole-checkerboard interaction classification

3.3 Efflux phenotype

Mean EtBr fluorescence was 1497.5 ± 660.0, 4701.7 ± 502.4 and 5686.2 ± 733.5 for control, CuO and CCCP in K. pneumoniae, and 1446.4 ± 472.0, 5162.9 ± 376.4 and 6192.7 ± 515.3 in P. aeruginosa. Median CuO-associated changes were 242.2% (176.6–300.0) and 265.7% (218.4–328.7), respectively. Recalculated between-species Welch comparisons gave P = 0.626 for control, P < 0.001 for CuO and P < 0.001 for CCCP. Thus, the non-significant control contrast does not imply absence of species differences under treatment. The joint Wald test of treatment-associated fluorescence changes was significant (P = 0.002).

Table 3. Species × treatment analysis of ethidium bromide accumulation

Species	Control mean ± SD	CuO mean ± SD	CCCP mean ± SD	CuO change % median (IQR)
K. pneumoniae	1497.5 ± 660.0	4701.7 ± 502.4	5686.2 ± 733.5	242.2 (176.6–300.0)
P. aeruginosa	1446.4 ± 472.0	5162.9 ± 376.4	6192.7 ± 515.3	265.7 (218.4–328.7)

The between-species control comparison was non-significant (Welch P = 0.626), whereas mean fluorescence differed under CuO and CCCP (both P < 0.001). The two-contrast Wald test supported differing treatment-associated changes between species (P = 0.002). Kp_14 and Pa_19 showed lower EtBr retention and increased efflux-associated gene expression after CuO exposure and remained in the analysis.

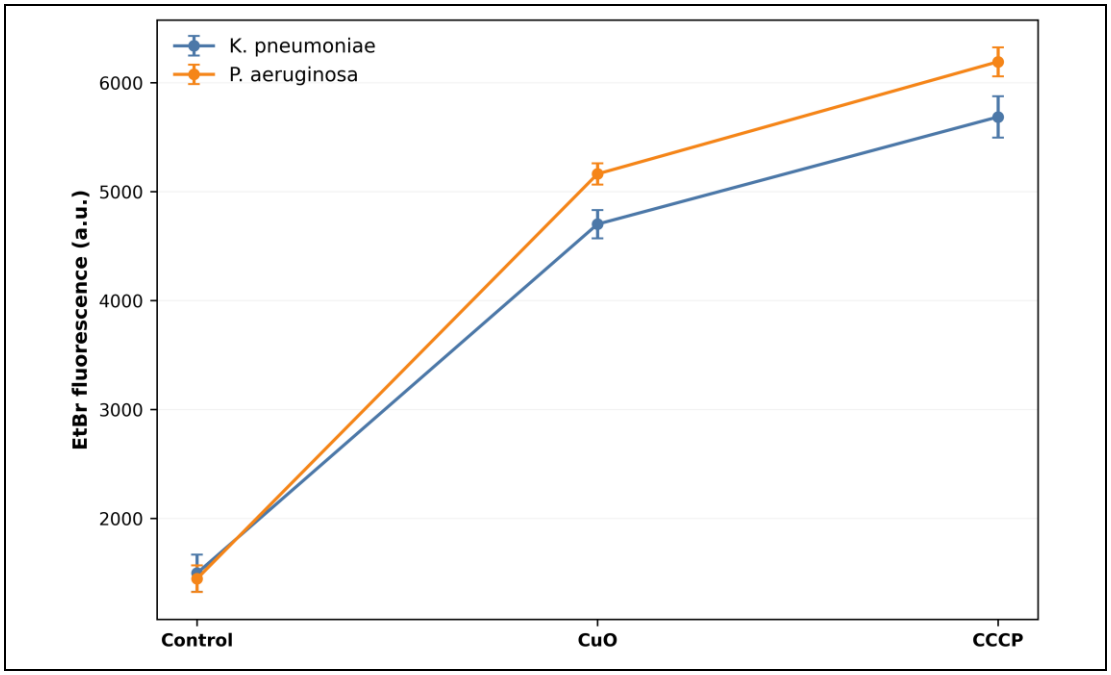

Figure 3. Ethidium bromide accumulation under control, CuO nanoparticle and CCCP conditions according to bacterial species.

The predominant ordering of EtBr fluorescence was control < CuO < CCCP. The Species × Treatment interaction indicates that the magnitude of the response differed between species; the control comparison alone does not establish absence of species differences under treatment. EtBr accumulation measures net intracellular retention, which depends on uptake, permeability and efflux. Increased fluorescence is therefore compatible with reduced efflux, but is not a specific demonstration of pump inhibition.

3.4 Transcriptional response

All eight targets had lower cohort median expression after CuO exposure. In *K. pneumoniae*, median fold changes were 0.390 (0.313–0.453) for *acrA*, 0.429 (0.355–0.476) for *acrB*, 0.405 (0.368–0.441) for *tolC* and 0.331 (0.253–0.412) for *ramA*. In *P. aeruginosa*, they were 0.411 (0.320–0.456) for *mexA*, 0.424 (0.349–0.477) for *mexB*, 0.378 (0.296–0.421) for *oprM* and 0.431 (0.330–0.484) for *mexR*. Between 58 and 59 of 60 isolates were downregulated for each gene, and every comparison survived Holm correction (P < 0.001). The effect spanned structural components and their regulators, but does not establish the causal mechanism.

Table 4. Relative expression of efflux pump-associated genes following CuO treatment

Species	Gene	Fold change median (IQR)	Downregulated n (%)	Test on ΔCt	Holm-adjusted P
K. pneumoniae	acrA	0.390 (0.313–0.453)	59 (98.3%)	Wilcoxon signed-rank	<0.001
K. pneumoniae	acrB	0.429 (0.355–0.476)	59 (98.3%)	Wilcoxon signed-rank	<0.001
K. pneumoniae	tolC	0.405 (0.368–0.441)	58 (96.7%)	Wilcoxon signed-rank	<0.001
K. pneumoniae	ramA	0.331 (0.253–0.412)	59 (98.3%)	Wilcoxon signed-rank	<0.001
P. aeruginosa	mexA	0.411 (0.320–0.456)	59 (98.3%)	Wilcoxon signed-rank	<0.001
P. aeruginosa	mexB	0.424 (0.349–0.477)	59 (98.3%)	Wilcoxon signed-rank	<0.001
P. aeruginosa	oprM	0.378 (0.296–0.421)	59 (98.3%)	Wilcoxon signed-rank	<0.001
P. aeruginosa	mexR	0.431 (0.330–0.484)	59 (98.3%)	Wilcoxon signed-rank	<0.001

After multiplicity correction, all eight prespecified efflux associated genes showed significant treatment related changes. The median fold change for K. pneumoniae ranged from 0.331 (ramA) to 0.429 (acrB) with 58–59/60 isolates with < 1.0 for each gene. The median fold changes for P. aeruginosa were: oprM (0.378) and mexR (0.431) with 59 out of 60 isolates showing lower expression of both genes. Because of this, the fold change values were not used in the statistical inference and 2^-ΔΔCt was kept for biological presentation. The over-riding pattern is thus that the whole gene-expression program associated with efflux is generally down regulated following exposure to CuO, except for two: Kp_14 and Pa_19 are more inclined to up than down.

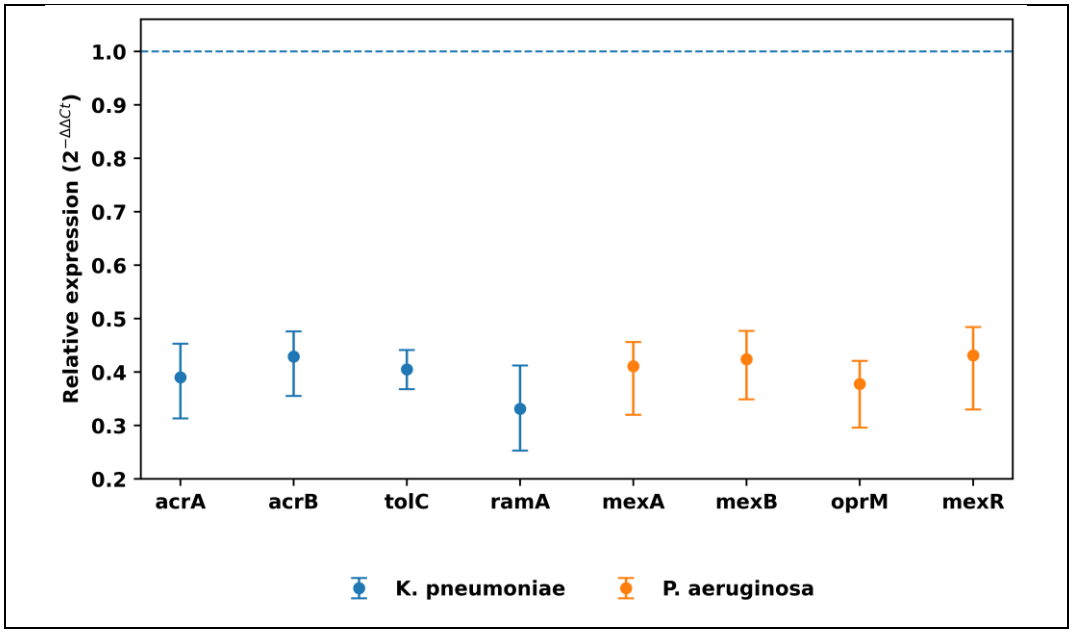

Figure 4. Relative expression of efflux pump-associated genes following sub-inhibitory CuO nanoparticle exposure.

Median expression of every measured target was below the unity line in both species. This is a cohort summary rather than a uniform response: individual reversals were retained in the analysis and are discussed separately. Lower transcript abundance is compatible with an efflux-related contribution but does not directly quantify pump protein abundance or transport activity.

3.5 Biofilm, time-kill and cytotoxicity

Biofilm inhibition was greater in *P. aeruginosa* (73.62%, 67.36–77.99) than *K. pneumoniae* (66.92%, 61.39–72.04; P < 0.001). The between-species comparison of within-isolate optical-density change gave P = 0.012. At 24 h, median additional killing with meropenem was 2.306 (2.286–2.335) and 2.295 (2.270–2.328) log10 CFU/mL, respectively (between-species P = 0.231). Ciprofloxacin values were 2.279 (1.328–2.317) and 2.275 (1.355–2.309) (P = 0.834). The pooled paired comparison was significant (P < 0.001), but differences between the meropenem and ciprofloxacin group medians were approximately 0.027 and 0.020 log10 CFU/mL in K. pneumoniae and P. aeruginosa, respectively; these are differences of medians rather than medians of paired isolate-level differences and do not establish biologically meaningful superiority. The narrow meropenem IQR describes the recorded across-isolate endpoints, not independent-repeat precision. Median CC50 estimates were 365.96 (186.48–476.22) and 383.22 (215.20–492.90) µg/mL (P = 0.562), with concentration ratios of 6.30 (5.57–7.09) and 6.18 (5.46–7.17) (P = 0.653). Mean viability was approximately 94%, 85%, 66% and 40% across 0.25, 0.5, 1 and 2 × MIC exposure levels. Ratios exceeded 1 in 119/120 series. Five CC50 estimates (3/60 K. pneumoniae and 2/60 P. aeruginosa) exceeded the maximum tested concentration of their respective series; these estimates require extrapolation beyond the measured dose range.

Table 5. Biofilm inhibition, recalculated additional killing and MIC-normalised cytotoxicity outcomes

Outcome	K. pneumoniae (n = 60)	P. aeruginosa (n = 60)	P value
Biofilm inhibition (%)	66.92 (61.39–72.04)	73.62 (67.36–77.99)	<0.001
MEM 24 h additional killing vs best single agent (log10 CFU/mL)	2.306 (2.286–2.335)	2.295 (2.270–2.328)	0.231
CIP 24 h additional killing vs best single agent (log10 CFU/mL)	2.279 (1.328–2.317)	2.275 (1.355–2.309)	0.834
CC50 CuO (µg/mL)	365.96 (186.48–476.22)	383.22 (215.20–492.90)	0.562
MIC-normalised ratio (CC50/[0.25 × CuO MIC])	6.30 (5.57–7.09)	6.18 (5.46–7.17)	0.653

Time-kill summaries in Table 5 were calculated from the recorded isolate-level 24-hour values: additional killing = the lower log10 CFU/mL value of the two single-agent conditions minus the combination value. The interquartile ranges describe between-isolate variation, not variability between independent experimental repeats. Their narrowness persists in the supplied endpoint data and does not establish assay reproducibility. CC50 estimates and concentration ratios are grouped by the bacterial MIC used to define the exposure grid in the same human-cell model; this grouping does not establish species-specific human-cell toxicity or clinical safety. Five CC50 estimates (Kp_11, Kp_33, Kp_55, Pa_22 and Pa_60) exceed their respective maximum tested doses and require extrapolation; the corresponding ratios inherit this uncertainty.

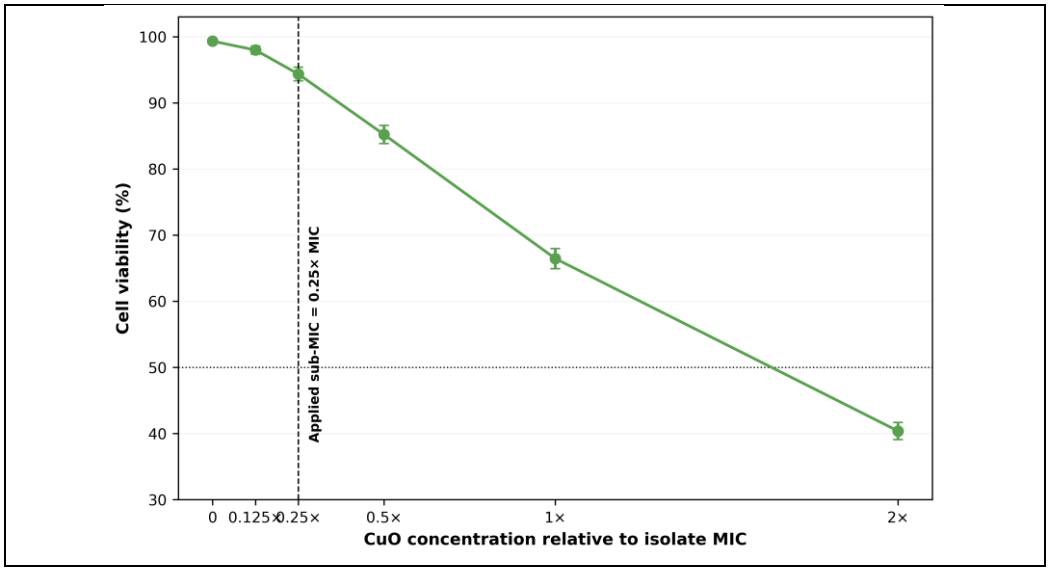

Figure 5. Cell viability across MIC-normalised CuO exposure levels.

Mean cell viability was approximately 94%, 85%, 66% and 40% at 0.25, 0.5, 1 and 2 × CuO MIC, respectively. These are aggregated MIC-normalised exposure levels: the same multiplier corresponds to different absolute concentrations for different bacterial isolates. The plot describes viability under this dosing scheme, rather than a single absolute-concentration toxicity curve. Neither its visual separation from 50% viability nor the reported concentration ratio validates a clinical safety margin.

3.6 Pooled and species-stratified exploratory correlations

The following Spearman correlations were calculated after pooling both species (n = 120). EtBr change was inversely correlated with mean efflux-gene fold change (ρ = −0.856) and positively correlated with biofilm inhibition (ρ = 0.887); mean fold change correlated inversely with biofilm inhibition (ρ = −0.710). Meropenem FICI correlated with EtBr change (ρ = −0.378), mean fold change (ρ = 0.350) and biofilm inhibition (ρ = −0.361). CuO MIC correlated with CC50 (ρ = 0.907) and CC50 with MIC-normalised concentration ratio (ρ = 0.424); all Holm-adjusted P < 0.001.

Table 6. Pooled exploratory Spearman correlations (n = 120); species-stratified results are in Table S3

Variable 1	Variable 2	Spearman ρ	Holm-adjusted P
EtBr change (%)	Mean efflux-gene fold change	-0.856	<0.001
EtBr change (%)	Biofilm inhibition (%)	0.887	<0.001
Mean efflux-gene fold change	Biofilm inhibition (%)	-0.710	<0.001
FICI Meropenem	EtBr change (%)	-0.378	<0.001

Variable 1	Variable 2	Spearman ρ	Holm-adjusted P
FICI Meropenem	Mean efflux-gene fold change	0.350	<0.001
FICI Meropenem	Biofilm inhibition (%)	-0.361	<0.001
CuO MIC	CC50	0.907	<0.001
CC50	MIC-normalised ratio	0.424	<0.001

Within K. pneumoniae, EtBr change correlated with mean gene fold change (ρ = −0.890) and biofilm inhibition (ρ = 0.861); corresponding coefficients within P. aeruginosa were −0.900 and 0.947. All remained significant after Holm correction. The gene-expression–biofilm associations were also inverse within both species (ρ = −0.808 and −0.847). Thus, these associations do not depend solely on between-species mean differences. In contrast, meropenem FICI associations with EtBr, gene expression and biofilm inhibition were significant in K. pneumoniae (ρ = −0.633, 0.616 and −0.571) but not in P. aeruginosa (ρ = −0.137, 0.104 and −0.207; Holm-adjusted P > 0.05). The pooled FICI associations should therefore not be generalised uniformly to both species.

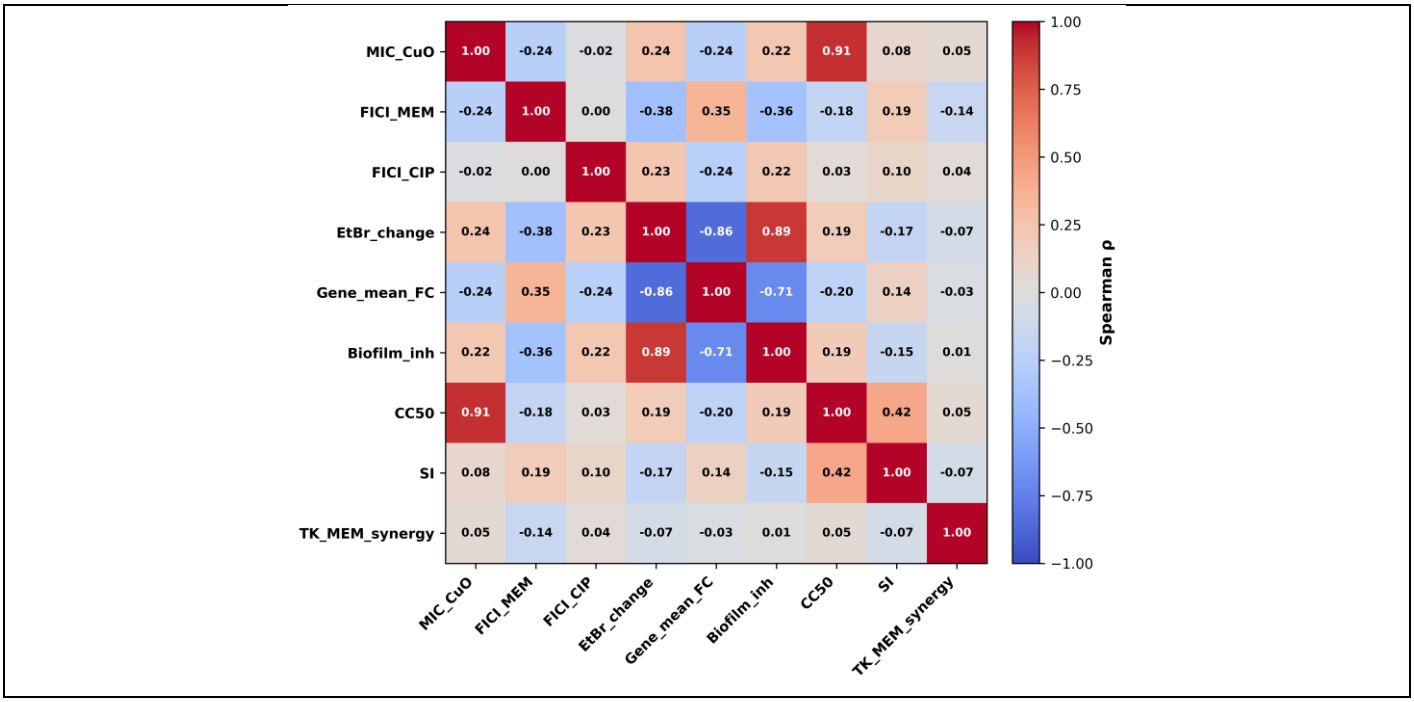

Figure 6. Exploratory correlation heatmap for the pooled two-species cohort (n = 120). The SI axis label denotes the MIC-normalised concentration ratio CC50/(0.25 × CuO MIC).

The heatmap displays pooled descriptive coefficients. Table S3 separately reports the prespecified within-species tests. In Figure 6, ciprofloxacin FICI correlates positively with EtBr change (ρ = 0.234) and biofilm inhibition (ρ = 0.217), and negatively with mean gene fold change (ρ = −0.238). These directions oppose the meropenem pattern: favourable

efflux-associated markers do not uniformly predict a lower FICI across antibiotic partners. Meropenem additional killing at 24 h is weakly correlated with EtBr change (ρ = −0.067), gene fold change (ρ = −0.030) and biofilm inhibition (ρ = 0.007). Thus, the killing endpoint does not provide a parallel correlation-based confirmation of the proposed mechanism. These additional heatmap coefficients are descriptive and were not added to the prespecified 24-test Holm family. The MIC–CC50 block remains partly design-dependent because MIC determined the cytotoxicity concentration grid.

3.7 Discordant isolates

Five isolates illustrate response heterogeneity. Kp_14 had a recorded meropenem FICI of 4.25 at CuO 576 µg/mL (2.25 × MIC), while its reduced EtBr retention and increased gene expression were measured at CuO 64 µg/mL (0.25 × MIC). These findings occurred under different exposure conditions and do not show that the efflux-associated response caused antagonism. Pa_19 had recorded FICI values of 0.375 with both antibiotics despite reduced EtBr retention and increased gene expression. Pa_48 showed gene downregulation with a × meropenem FICI of 1.50 (CuO 1 MIC) and a ciprofloxacin FICI of 0.375 (CuO 0.25 × MIC). Pa_59 had a × meropenem FICI of 0.50 (CuO 0.25 MIC) and a ciprofloxacin FICI of 1.50 (CuO 1 × MIC), together with a high ciprofloxacin MIC. Kp_55 showed a increase in biofilm rather than %42.7 inhibition. Separately, Kp_29 had low ,meropenem and ciprofloxacin MICs Pa_07 a high meropenem MIC and Pa_33 a low CuO MIC. All isolates ;remained in the numerical summaries endpoint classifications and mechanistic responses were not treated as measurements under identical .conditions

4. Discussion

4.1 Associations among efflux-related endpoints

Species-stratified analyses retained strong inverse EtBr–gene-expression associations (ρ = −0.890 in K. pneumoniae and −0.900 in P. aeruginosa) and positive EtBr–biofilm-inhibition associations (ρ = 0.861 and 0.947), all significant after Holm correction. These results address the concern that pooled associations might arise solely from differences between species. They do not establish causality. Importantly, FICI associations were significant only within K. pneumoniae, so antibiotic potentiation cannot be attributed to a uniform efflux-mediated pathway across the cohort. The opposite ciprofloxacin FICI directions and weak time-kill correlations in Figure 6 further limit mechanistic convergence across endpoints. In addition to permeability, stress and other copper effects, efflux and biofilm tolerance may also interact (Vareschi et al., 2025).

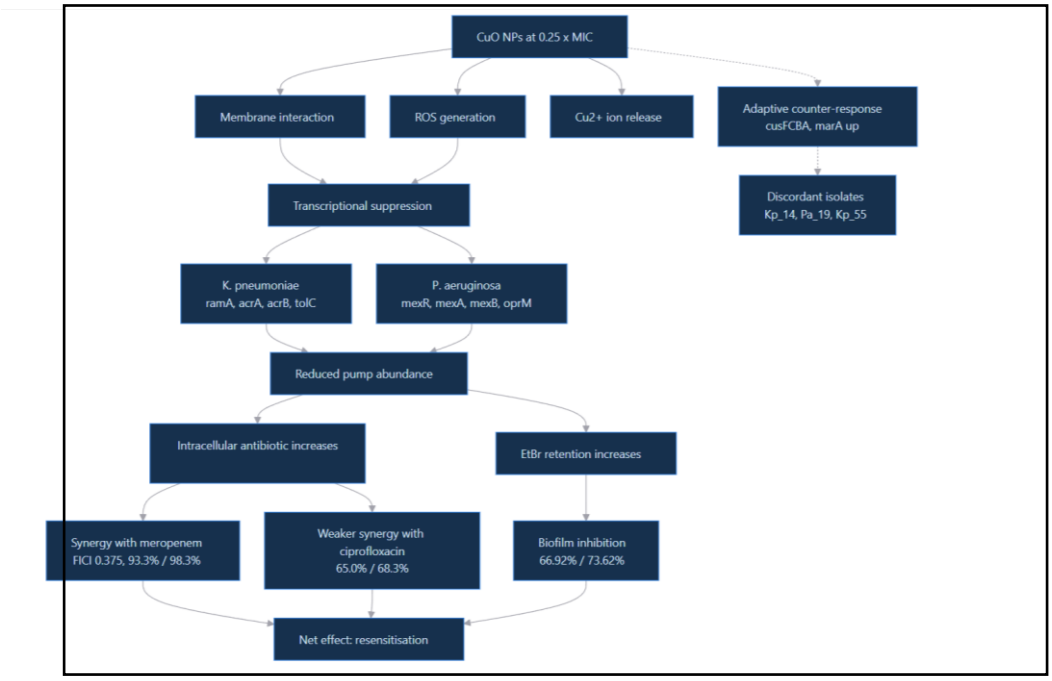

S2: Proposed CuO-related routes. Arrows represent hypotheses, not demonstrated causal steps. Reduced pump abundance and increased intracellular antibiotic concentrations were not measured. Terminal FICI labels summarise descriptive recorded endpoints at varying CuO fractions; they do not validate the proposed pathway or establish interactions at the diagram's 0.25 × MIC exposure.

4.2 Concordance with published work

Present associations are provided in the context of published work. Nanoparticle–membrane interactions and ions released contributions are described in reviews (Modi et al., 2023). It should be emphasized that a reduction in the expression of mexA gene was observed in resistant P. aeruginosa after CuO was added with chloramphenicol, this was a transcriptional measurement and not a measurement of actual numbers of MexA protein or active pumps (Alazavi et al., 2022). Afrasiabi and Partoazar (2024) review nanoparticle strategies targeting genes associated with biofilm. These reports do not prove that the mechanisms or efficacy between different types of particles is the same.

The transcription results are similar. Wang et al., 2022 quantified acrA, acrB and ramA genes (the same genes targeted in this study) and confirmed that AcrAB–TolC is an efflux determinant of resistance in K. pneumoniae. In P. aeruginosa, gold nanoparticles down-regulate mexA and mexB, but do not directly impact the number of functional pumps on the cell surface (Dorri et al., 2022). Our contribution is the assessment of these individual effects in the current two-species cohort, which showed that there was a decrease in median expression of structural and regulatory genes, but the response was variable. This is important mechanistically since ramA is the activator which upregulates acrAB and tolC (Han et al., 2022), and the simultaneous suppression of ramA along with acrAB and tolC is

compatible with a transcriptional contribution, although not excluding physical membrane effects, in K. pneumoniae. The result of P. aeruginosa is less clear-cut: mexR is the repressor of mexAB-oprM, so its decreased expression is expected to lead to a derepression of the pump, not to its decrease. This concordant MexR fall with mexA, mexB and oprM consequently suggests a transcriptional effect (or co-regulation across the operon) and this should be confirmed by direct testing.

Antibiofilm effects and Nanoparticle–antibiotic potentiation have been observed in other formulations and experimental systems such as silver nanoparticles with imipenem (Fontoura et al., 2023), meropenem–ZnO combination (Mohamed et al., 2024), and silver or copper nanoparticles against clinical bacterial biofilms (Elshaer & Shaaban, 2023). A different species of the K. pneumoniae group studied here was K. quasipneumoniae, which was studied by Devi et al. (2025). Due to differences in organism, formulation, concentration and endpoint, quantitative equivalences cannot be directly determined. This CuO exposure design resulted in the present biofilm inhibition and further killing; it is not evidence of superiority over those formulations.

4.3 Alternative explanations and context

Several observations require cautious interpretation.

In both species, the mean EtBr accumulation was higher for CCCP than for CuO (5686.2 vs. 4701.7; 6192.7 vs. 5162.9). It was not expected that the agents will be of equal potency. Increased retention, however, does not distinguish the mechanism: this may be due to increased efflux, increased membrane permeability, or both. It is not determined that CuO works via the same protonophore response.

More recorded meropenem FICI points met the synergy threshold than ciprofloxacin points; this comparison is conditional on the recorded endpoint selection. This difference cannot be explained solely by both antibiotic classes being efflux substrates (Gauba & Rahman, 2023). Another way through which an increase in the uptake of antibiotics can be achieved is by altering the permeability of the outer-membrane (Saxena et al., 2023). Another possibility is the copper-mediated inhibition of metallo-β-lactamases: the coumarin–copper complex GluC-Cu inhibited NDM-1, IMP-1 and ImiS and improved the activity of meropenem in another experimental system (Chen et al., 2023). This evidence concerns that copper complex, not proof that the preparation of the CuO used in this study inhibited those enzymes. In this study, copper release, membrane permeability, enzyme activity were not directly measured and detection of the carbapenemase-gene does not prove enzyme inhibition. The difference may also be attributed to quinolone-specific resistance determinants. Therefore, efflux inhibition alone should not be blamed for preferential meropenem potentiation.

Carbapenemase frequencies must be interpreted in relation to selection criteria and denominators. The present cohort was selected from isolates reported as multidrug resistant; frequencies should not be equated with prevalence in an unselected clinical population. Regional variation in carbapenemase distributions is also documented (Gracia-Ahufinger et al., 2023; Tuhamize & Bazira, 2024).

Fourth, blaKPC was only present in K. pneumoniae in our cohort, while

blaKPC is found in a significant number of carbapenem-resistant P. aeruginosa isolates in other cohorts (Mohamed et al., 2023). This is more of an epidemiological, not biological, disagreement. Similarly, in Spain, national mapping revealed that OXA-48-like enzymes are more common in Enterobacterales than VIM (Gracia-Ahufinger et al., 2023), and in Ecuador, blaKPC, blaNDM and blaOXA-48 were more prevalent than blaVIM in Enterobacterales (Soria-Segarra et al., 2024). A similar species weighting has been observed in cohorts from Iraq (Al-Hasso, 2022), United Arab Emirates (UAE) (Sharief et al., 2025), intensive-care burn units (ICU) (Haider et al., 2022) and systematic reviews (Tuhamize & Bazira, 2024) of carbapenem-resistant Enterobacterales from human, livestock and environmental samples. Our cohort follows this species weighting for blaKPC, blaOXA-48 and blaVIM. One caveat arises from the same data: blaNDM was disseminated at similar rates in both species (55.0% and 48.3%) and we did not screen for blaIMP, which is a recognised caveat as IMP-type enzymes are important in some settings locally (Kumar et al., 2025). The observation of similar MICs with different genotypes reiterates a methodological principle: Phenotype and genotype are complementary, not interchangeable. Porin-mediated permeability changes could also contribute to susceptibility differences, but porin expression and function were not measured in this cohort.

4.4 Discordant isolates and response heterogeneity

All five isolates remained in the numerical analyses. Kp_14 combines an outlying recorded FICI point with an ,opposite efflux-associated phenotype but these measurements used CuO concentrations differing ninefold. Its FICI cannot establish antagonism at the .mechanistic 0.25 × MIC exposure Pa_19 demonstrates that a recorded low FICI can coexist with reduced EtBr retention and increased gene expression. Pa_48 and Pa_59 illustrate antibiotic-specific threshold categories at different CuO fractions; they are not proof of intrinsic non-responsiveness at a matched dose. Kp_55 increased biofilm formation by 42.7%. The descriptive FICI selection, unmatched exposures and heterogeneous responses prevent a uniform mechanistic interpretation. Adaptive & responses are possible (Kamat ,Kumari, 2023), but mutations nanoresistance and causal regulatory .pathways were not demonstrated here

4.5 MIC-normalised cytotoxicity and translational interpretation

Median CC50 estimates were 365.96 and 383.22 µg/mL, and median CC50/(0.25 × CuO MIC) ratios were 6.30 and 6.18; 119/120 ratios exceeded 1. These summaries were grouped by the bacterial MIC used to set the exposure series, although the human cell model remained unchanged. Five CC50 estimates lie above their respective maximum tested doses, so their concentration ratios also depend on extrapolation. Neither the cohort summaries nor those extrapolated estimates establish isolate-specific human-cell toxicity or an independent safety margin. Mean viability of approximately 94% at 0.25 × MIC is encouraging within the tested conditions but does not establish clinical safety. Published CuO work also indicates formulation-dependent cytotoxicity (El-Kattan et al., 2025; Flores-Rábago *et al.,* 2023); results from other formulations or cell models cannot *validate* the present preparation.

Two constraints temper enthusiasm. Biofilm-directed nanoparticle therapy still requires systematic clinical validation before it

can be made available (Mohanta *et al.,* 2023), so the biofilm inhibition observed here at 0.25 × MIC, while substantial, should not be equated with eradication. And despite sustained effort, no efflux-pump inhibitor has progressed into clinical use, largely because of formulation, toxicity and pharmacokinetic limitations or narrow spectra of inhibition (Duffey *et al.,* 2024); standardised diagnostic and inhibitory approaches for efflux are still lacking (Rouvier *et al.,* 2025), and nanocarrier-based efflux inhibition faces additional barriers in safety, scale-up and bacterial adaptation (Mbara *et al.,* 2026). These in vitro associations motivate mechanistic testing; they do not establish a specific causal pathway or clinical efficacy.

4.6 Limitations

This single-centre in vitro experimental study used clinical isolates; the molecular panel excluded *bla*IMP, and regulator, quinolone-resistance and porin mechanisms were not characterised. Net EtBr retention cannot separate efflux from permeability, and copper release or enzyme inhibition was not measured. Mechanistic assays used 0.25 × MIC CuO (1–128 µg/mL across isolates), whereas recorded combination-MIC and response-matrix analyses varied CuO; these datasets should not be equated. The full concentration layout, inhibitory-well calls and minimum/maximum selection rule for the recorded FICI endpoints are not documented. The 4 × 4 response matrices neither contain all recorded FICI concentration pairs nor reproduce the single-agent MIC endpoint at their nominal 1 × MIC labels. Consequently, recorded FICI threshold categories remain descriptive, and Kp_14's 4.25 value does not independently verify checkerboard-wide or sub-MIC antagonism. Species-stratified associations address pooling effects but do not establish causal or species-adjusted treatment effects. Time-kill endpoint differences and quartiles can be recalculated, but antibiotic doses, independent repeat structure and replicate-level colony counts are not documented; the narrow IQR therefore does not establish repeatability. Final viable inoculum counts are not documented, and the reported 1:1000 preparation does not establish reference broth-microdilution density. Clinical susceptibility interpretations consequently require inoculum verification. EtBr results apply to the reported 40 °C condition without a reported 37 °C validation. The multiplex-PCR thermal program is not reported. MIC-normalised cytotoxicity curves and concentration ratios remain design-dependent. Five CC50 estimates exceed their respective maximum tested doses and require extrapolation; the original fitting procedure and parameter uncertainty are not documented. These estimates and ratios cannot establish a clinical safety margin.

5. Conclusions

More recorded meropenem FICI points met the ≤ 0.5 threshold than ciprofloxacin points, but these selected endpoint categories were not independently verified across complete checkerboards or at a common CuO dose. Bliss and HSA scores were reproduced from separate percent-inhibition matrices and do not validate the recorded FICI points. Median additional killing at 24 h was similar between antibiotic combinations. EtBr retention, gene expression and biofilm inhibition were associated within both species; however, antibiotic-specific FICI patterns, weak time-kill correlations and exposure differences prevent a uniform causal interpretation. Kp_14's 4.25 FICI is an outlying recorded point at supra-MIC CuO, not established antagonism at the mechanistic 0.25 × MIC dose. MIC-

normalised cytotoxicity ratios remain exploratory and do not establish clinical safety.

Declarations

Ethical approval: [The author must supply the ethics committee name and approval/reference number before resubmission.]

Funding: This research received no external funding and was self-funded by the researcher.

Conflicts of interest: The author declares no conflict of interest.

Data availability: The data supporting this study are available from the corresponding author on reasonable request.

References

Afrasiabi, S., & Partoazar, A. (2024). Targeting bacterial biofilm-related genes with nanoparticle-based strategies. *Frontiers in Microbiology*, *15*, 1387114. https://doi.org/10.3389/fmicb.2024.1387114

Alazavi, F., Molavi, F., & Tehranipoor, M. (2022). Synergistic effect of copper oxide nanoparticles and chloramphenicol antibiotic on MexA gene expression of pump efflux system in drug-resistant Pseudomonas aeruginosa isolates. *Medical Journal of Tabriz University of Medical Sciences*, *44*(2), 127–138. https://doi.org/10.34172/mj.2022.022

Al-Hasso, M. Z. (2022). Determination of antimicrobial resistance profiles and molecular detection of carbapenemases in Gram negative bacilli isolated from different sources in Mosul city, Iraq. *Kuwait Journal of Science*. https://doi.org/10.48129/kjs.17079

Blinov, A., Gvozdenko, A. A., Golik, A. B., Blinova, A. A., Slyadneva, K. S., Pirogov, M. A., & Maglakelidze, D. G. (2022). Synthesising Copper Oxide Nanoparticles and Investigating the Effect of Dispersion Medium Parameters on their Aggregate Stability. *Herald of the Bauman Moscow State Technical University. Series Natural Sciences*, *2022*(4), 95–109. https://doi.org/10.18698/1812-3368-2022-4-95-109

Chen, C., Li, J., Dan, H., He, J., Wang, D., Oelschlaeger, P., Wang, N., Zhang, Y., Pei, Y., & Yang, K.-W. (2023). A self-reported inhibitor of metallo-carbapenemases for reversing carbapenem resistance. International Journal of Biological Macromolecules, 252, 126441. https://doi.org/10.1016/j.ijbiomac.2023.126441

Devi, A., Kaundal, R. K., Gupta, N., Kumar, D., Singh, R. P., & Kaur, T. (2025). Antibacterial and antibiofilm activity of nanoparticles in Klebsiella quasipneumoniae. *RSC Advances*, *15*(51), 43576–43594. https://doi.org/10.1039/d5ra04828a

Dorri, K., Modaresi, F., Shakibaie, M. R., & Moazamian, E. (2022). Effect of gold nanoparticles on the expression of efflux pump mexA and mexB genes of Pseudomonas aeruginosa strains

by Quantitative real-time PCR. *Pharmacia*, *69*(1), 125–133. https://doi.org/10.3897/pharmacia.69.e77608

Duffey, M., Jumde, R. P., Costa, R. M. A. da, Ropponen, H., Blasco, B., & Piddock, L. J. V. (2024). Extending the Potency and Lifespan of Antibiotics: Inhibitors of Gram-Negative Bacterial Efflux Pumps. *ACS Infectious Diseases*, *10*(5), 1458–1482. https://doi.org/10.1021/acsinfecdis.4c00091

El-Kattan, N., Ibrahim, M., Emam, A. N., Khaled, M., Youssef, F. S., Nassar, N. A., & Mansour, A. S. (2025). Evaluation of the antimicrobial activity of chitosan- and curcumin-capped copper oxide nanostructures against multi-drug-resistant microorganisms. *Nanoscale Advances*, *7*(10), 2988–3007. https://doi.org/10.1039/d4na00955j

Elshaer, S. L., & Shaaban, M. I. (2023). Antibiofilm activity of biosynthesized silver and copper nanoparticles using Streptomyces S29. *AMB Express*, *13*(1), 139. https://doi.org/10.1186/s13568-023-01647-3

European Committee on Antimicrobial Susceptibility Testing (EUCAST). (2024). EUCAST reading guide for broth microdilution. Version 5.0. https://www.eucast.org/bacteria/methodology-and-instructions/mic-determination/

Flores-Rábago, K. M., Rivera-Mendoza, D., Vilchis-Néstor, A. R., Juárez-Moreno, K., & Castro-Longoria, E. (2023). Antibacterial Activity of Biosynthesized Copper Oxide Nanoparticles (CuONPs) Using Ganoderma sessile. *Antibiotics*, *12*(8), 1251. https://doi.org/10.3390/antibiotics12081251

Fontoura, I., Veriato, T. S., Raniero, L., & Castilho, M. L. (2023). Analysis of Capped Silver Nanoparticles Combined with Imipenem against Different Susceptibility Profiles of Klebsiella pneumoniae. *Antibiotics*, *12*(3), 535. https://doi.org/10.3390/antibiotics12030535

Garcia-Maset, R., Chu, V., Yuen, K. Y., Blumgart, D., Yoon, J., Murray, B., Joseph, A. A., & Rohn, J. (2025). Effect of host microenvironment and bacterial lifestyles on antimicrobial sensitivity and implications for susceptibility testing. *Npj Antimicrobials and Resistance*, *3*(1), 42. https://doi.org/10.1038/s44259-025-00113-3

Gauba, A., & Rahman, K. M. (2023). Evaluation of Antibiotic Resistance Mechanisms in Gram-Negative Bacteria. *Antibiotics*, *12*(11), 1590. https://doi.org/10.3390/antibiotics12111590

GBD 2021 Antimicrobial Resistance Collaborators. (2024). Global burden of bacterial antimicrobial resistance 1990–2021: a systematic analysis with forecasts to 2050. The Lancet, 404(10459), 1199–1226. https://doi.org/10.1016/S0140-6736(24)01867-1

Gracia-Ahufinger, I., López-González, L., Vasallo, F. J., Galar, A., Siller, M., Pitart, C., Bloise, I., Torrecillas, M., Gijón-Cordero,

D., Viñado, B., Castillo-García, J., Campo, R., Mulet, X., Madueño-Alonso, A., Chamizo-López, F. J., Arrastia-Erviti, M., Galán-Sánchez, F., Fernández-Quejo, M., Rodríguez, J. C., … Martínez-Martínez, L. (2023). The CARBA-MAP study: national mapping of carbapenemases in Spain (2014–2018). *Frontiers in Microbiology*, *14*. https://doi.org/10.3389/fmicb.2023.1247804

Gudkov, S. V., Burmistrov, D. E., Fomina, P. A., Validov, S., & Kozlov, V. A. (2024). Antibacterial Properties of Copper Oxide Nanoparticles (Review). *International Journal of Molecular Sciences*, *25*(21), 11563. https://doi.org/10.3390/ijms252111563

Haider, M. H., McHugh, T. D., Roulston, K., Arruda, L. B., Sadouki, Z., & Riaz, S. (2022). Detection of carbapenemases blaOXA48-blaKPC-blaNDM-blaVIM and extended-spectrum-β-lactamase blaOXA1-blaSHV-blaTEM genes in Gram-negative bacterial isolates from ICU burns patients. *Annals of Clinical Microbiology and Antimicrobials*, *21*(1), 18. https://doi.org/10.1186/s12941-022-00510-w

Hajiagha, M. N., & Kafil, H. S. (2023). Efflux pumps and microbial biofilm formation. *Infection Genetics and Evolution*, *112*, 105459. https://doi.org/10.1016/j.meegid.2023.105459

Han, Y., Wen, X., Zhao, W., Cao, X., Wen, J.-X., Wang, J., Hu, Z., & Zheng, W. (2022). Epidemiological characteristics and molecular evolution mechanisms of carbapenem-resistant hypervirulent Klebsiella pneumoniae. *Frontiers in Microbiology*, *13*, 1003783. https://doi.org/10.3389/fmicb.2022.1003783

Hussein, R. A., Al-Kubaisy, S. H. M., & Al-Ouqaili, M. T. S. (2024). The influence of efflux pump, outer membrane permeability and β-lactamase production on the resistance profile of multi, extensively and pandrug resistant Klebsiella pneumoniae. *Journal of Infection and Public Health*, *17*(11), 102544. https://doi.org/10.1016/j.jiph.2024.102544

Ianevski, A., Giri, A. K., & Aittokallio, T. (2022). SynergyFinder 3.0: an interactive analysis and consensus interpretation of multi-drug synergies *across multiple samples. Nucleic Acids Research*, 50(W*1)*, W739–W743. https://doi.org/10.1093/nar/gkac382

Kamat, S., & Kumari, M. (2023). Emergence of microbial resistance against nanoparticles: Mechanisms and strategies. *Frontiers in Microbiology*, *14*, 1102615. https://doi.org/10.3389/fmicb.2023.1102615

Kumar, D., Chaudhary, M., Gadepalli, R., Vaishnavi, M., Aggarwal, A., Tak, V., Bohra, G. K., Meena, D. S., Midha, N. K., Samantaray, S., Solanki, H., Kothari, N., Bhatia, P., & Garg, M. (2025). P-1354. Carbapenemase Gene Detection in Clinically Significant Pseudomonas aeruginosa Isolates from A Tertiary Care Health Center: A Prospective Study.

Open Forum Infectious Diseases, *12*. https://doi.org/10.1093/ofid/ofae631.1531

Mbara, K. C., Ngcobo, Y., Chivasa, B., Masemola, L., Mashamaite, R., Mokhetho, K. C., Phuthi, M., Mangisa, M., Kheoane, P. S., Mokhele, S., Marakalala, L. M., Mbeb, C. N., Emeyene, R. P., Leonard, C. M., Tembu, V. J., & Tarirai, C. (2026). Fighting back against bacterial resistance: Harnessing nanocarrier strategies to counter antibiotic efflux pumps. *Next Materials*, *10*, 101540. https://doi.org/10.1016/j.nxmate.2025.101540

Modi, S. K., Gaur, S., Sengupta, M., & Singh, M. S. (2023). Mechanistic insights into nanoparticle surface-bacterial membrane interactions in overcoming antibiotic resistance. *Frontiers in Microbiology*, *14*, 1135579. https://doi.org/10.3389/fmicb.2023.1135579

Mohamed, A. A., Saed, S., Elsayed, S., Yassin, M. T., Gad, M., Tartour, E., Fathey, H. A., Taha, A. S., Mohamed, A. H., Al-Otibi, F. O., AbdelGawwad, M. R., Ahmed, M., Almalki, S. A., & Abdel-Haleem, M. (2024). A combined therapy of meropenem–ZnO nanoparticles efficiently eliminates carbapenem-resistant Klebsiella pneumoniae biofilms, with reduced nephrotoxicity (in vitro). *Letters in Applied Microbiology*, *77*(12). https://doi.org/10.1093/lambio/ovae136

Mohamed, S., Ahmed, Z. S. O., Mubarak, T., Mohamed, S., Mohamed, R., Higazi, H., & Ali, S. (2023). Co-occurrence of Carbapenemase Genes blaNDM, blaVIM, blaKPC and blaOXA-48 in Pseudomonas aeruginosa Clinical Isolates. *International Journal of Biomedicine*, *13*(3), 123–126. https://doi.org/10.21103/article13(3)_oa12

Mohanta, Y. K., Chakrabartty, I., Mishra, A. K., Chopra, H., Mahanta, S., Avula, S. K., Patowary, K., Ahmed, R., Mishra, B., Mohanta, T. K., Saravanan, M., & Sharma, N. (2023). Nanotechnology in combating biofilm: A smart and promising therapeutic strategy. *Frontiers in Microbiology*, *13*, 1028086. https://doi.org/10.3389/fmicb.2022.1028086

Mudenda, S., Hakayuwa, C. M., Lubanga, A. F., Kasanga, M., Daka, V., Salachi, K. I., Mwaba, M., Chileshe, C., Champo, M., Kamayani, M., Harawa, G., Bwanali, A. N., Sinyawa, T., Hangoma, J., Simweene, C., Kanaan, M. H. G., Mugenyi, N., Chizimu, J. Y., Mohamed, S., … Muma, J. B. (2025). Global Antimicrobial Stewardship, Surveillance, and Infection Prevention and Control Programs: Leveraging One Health, Nanotechnology, and Artificial Intelligence to Combat Antimicrobial Resistance in a Climate-Impacted World. *Pharmacology & Pharmacy*, *16*(7), 197–291. https://doi.org/10.4236/pp.2025.167014

Rouvier, F., Brunel, J. M., Pagès, J., & Vergalli, J. (2025). Efflux-Mediated Resistance in Enterobacteriaceae: Recent Advances and Ongoing Challenges to Inhibit Bacterial

Efflux Pumps. *Antibiotics*, *14*(8), 778. https://doi.org/10.3390/antibiotics14080778

Sartorius, B., Gray, A. P., Weaver, N. D., Aguilar, G. R., Swetschinski, L. R., Ikuta, K. S., Meštrović, T., Chung, E., Wool, E. E., Han, C., Hayoon, A. G., Araki, D. T., Abd-Elsalam, S., Aboagye, R. G., Adamu, L. H., Adepoju, V. A., Ahmed, A., Akalu, G. T., Akande-Sholabi, W., … Naghavi, M. (2024). The burden of bacterial antimicrobial resistance in the WHO African region in 2019: a cross-country systematic analysis. *The Lancet Global Health*, *12*(2), e201–e216. https://doi.org/10.1016/s2214-109x(23)00539-9

Sati, H. F., Carrara, E., Savoldi, A., Hansen, P., Garlasco, J., Campagnaro, E., … Tacconelli, E. (2025). The WHO Bacterial Priority Pathogens List 2024: a prioritisation study to guide research, development, and public health strategies against antimicrobial resistance. *The Lancet Infectious Diseases*, *25(9)*, 1033–1043. https://doi.org/10.1016/S1473-3099(25)00118-5

Saxena, D., Maitra, R., Bormon, R., Czekańska, M., Meiers, J., Titz, A., Verma, S., & Chopra, S. (2023). Tackling the outer membrane: facilitating compound entry into Gram-negative bacterial pathogens. *Npj Antimicrobials and Resistance*, *1*(1), 17. https://doi.org/10.1038/s44259-023-00016-1

Sharief, H. E., Ali, S. M., Mohamed, S., Abbas, N., Maher, M., Kumar, P., & Elnour, S. (2025). Prevalence of Carbapenemase Genes blaOXA-48, blaNDM, and blaIMP in Multidrug Resistant Pseudomonas aeruginosa and Klebsiella pneumoniae Clinical Isolates from University Hospital Sharjah, UAE. *International Journal of Biomedicine*, *15*(4). https://doi.org/10.21103/article15(4)_oa14

Sobhanipoor, M. H., Ahmadrajabi, R., Hosseini-Nave, H., & Saffari, F. (2022). Determination of efflux activity in Enterococci by Hoechst accumulation assay and the role of zinc oxide nanoparticles in inhibition of this activity. *BMC Microbiology*, *22*(1), 195. https://doi.org/10.1186/s12866-022-02595-x

Soria-Segarra, C., Soria-Segarra, C., Molina-Matute, M., Agreda-Orellana, I., Núñez-Quezada, T., Cevallos-Apolo, K., Miranda-Ayala, M., Salazar-Tamayo, G., Galarza-Herrera, M., Vega-Hall, V., Villacís, J. E., & Gutiérrez-Fernández, J. (2024). Molecular epidemiology of carbapenem-resistant gram-negative bacilli in Ecuador. *BMC Infectious Diseases*, *24*(1), 378. https://doi.org/10.1186/s12879-024-09248-6

Thillai, B. D., Kini, S., & Deekshit, V. K. (2025). Nanobiotics to tackle efflux-mediated resistance in bacterial pathogens. *Critical Reviews in Microbiology*, 554–576. https://doi.org/10.1080/1040841x.2025.2597220

Tuhamize, B., & Bazira, J. (2024). Carbapenem-resistant Enterobacteriaceae in the livestock, humans and environmental samples around

the globe: a systematic review and meta-analysis. *Scientific Reports*, *14*(1), 16333. https://doi.org/10.1038/s41598-024-64992-8

Vareschi, S., Jaut, V., Vijay, S., Allen, R. J., & Schreiber, F. (2025). Antimicrobial efflux and biofilms: an interplay leading to emergent resistance evolution. *Trends in Microbiology*, *33*(9), 1018–1032. https://doi.org/10.1016/j.tim.2025.04.012

Wang, X., Xu, X., Zhang, S., Chen, N., Sun, Y., Ma, K., Hong, D., Li, L., Du, Y., Lu, X., & Jiang, S. (2022). TPGS-based and S-thanatin functionalized nanorods for overcoming drug resistance in Klebsiella pneumonia. *Nature Communications*, *13*(1), 3731. https://doi.org/10.1038/s41467-022-31500-3

Supplementary Tables

Supplementary Table S1. Multiplex PCR primer sequences and expected amplicon sizes for carbapenemase genes.

Gene	Forward primer (5′→3′)	Reverse primer (5′→3′)	Expected amplicon size
blaKPC	TGTCACTGTATCGCCGTCTA	AGACGACGGCATAGTCATTT	747 bp
blaNDM	GCAGCACACTTCCTATCTCG	CGGTGATATTGTCACTGGTGT	410 bp
blaVIM	TGGTGATGAGTTGCTTTTGA	GCAGCACCAGGATAGAAGAG	306 bp
blaOXA-48	GCGTAGTTGTGCTCTGGAAT	GGGCATATCCATATTCATCG	602 bp

Note: The multiplex-PCR thermal cycling program is not reported. Primer sequences and expected amplicon sizes alone do not specify a reproducible amplification protocol.

Supplementary Table S2. RT-qPCR primer sequences and species-specific reference genes.

Species	Gene	Forward primer (5′→3′)	Reverse primer (5′→3′)
K. pneumoniae	acrA	GCCTATCGCATTGCGGAAG	TTGGCGCTGTCATAGCTGG
K. pneumoniae	acrB	GGAAGCGATCATCCTGGTGTT	ACCGCGAAGGTGCCTAACA
K. pneumoniae	tolC	TACCAGCAGGCACGCATCA	GCTGTCGCGATAGCCATTGT
K. pneumoniae	ramA	TGCATCAACCGCTGCGTAT	GCGAATCAAAGCCATACTTGAG
K. pneumoniae	rpoB	GGTAATTCCGAGCTGCAATACG	CGCGCTCGTAGATCACCAG
P. aeruginosa	mexA	ATTCTCCGAGGTTTCCGTCG	AGGATGGCCTTCTGCTTGAC
P. aeruginosa	mexB	AGGAAAGCTCTTCGGTCAGC	GCTTGAGCATGATGAACGCC
P. aeruginosa	oprM	TTCGGGTTCCTGGTTGTTCC	TGTCCTTCTGGATCTTCGCG
P. aeruginosa	mexR	GAGGGAAGAAACCTGGTCCG	GGGGCAAACAACTCGTCATG
P. aeruginosa	rpoD	GCGGATGATGTCTTCCACCTGTTCC	GCGCAACAGCAATCTCGTCTGAAAGA

Note: rpoB was the reference gene for K. pneumoniae and rpoD for P. aeruginosa; the two genes were not used jointly within either species. Primer sequences are reproduced from the experimental documentation. The first documented rpoB primer pair was retained.

Supplementary Table S3. Species-stratified Spearman correlations (n = 60 per species).

Variable pair	K. pneumoniae ρ	Holm-adjusted P	P. aeruginosa ρ	Holm-adjusted P
EtBr change / mean gene fold change	-0.890	<0.001	-0.900	<0.001
EtBr change / biofilm inhibition	0.861	<0.001	0.947	<0.001
Mean gene fold change / biofilm inhibition	-0.808	<0.001	-0.847	<0.001
Meropenem FICI / EtBr change	-0.633	<0.001	-0.137	0.590

Variable pair	K. pneumoniae ρ	Holm-adjusted P	P. aeruginosa ρ	Holm-adjusted P
Meropenem FICI / mean gene fold change	0.616	<0.001	0.104	0.590
Meropenem FICI / biofilm inhibition	-0.571	<0.001	-0.207	0.338
CuO MIC / CC50	0.873	<0.001	0.934	<0.001
CC50 / MIC-normalised ratio	0.583	<0.001	0.278	0.125

Note: Mean gene fold change is the mean of the four species-specific targets. Holm correction covers all 24 correlation tests (eight pairs in the pooled cohort and each species). CC50 ratio = CC50/(0.25 × CuO MIC). These exploratory associations do not establish causality.